Enforcing passivity of parameterized LTI macromodels via Hamiltonian-driven multivariate adaptive sampling

Enforcing passivity of parameterized LTI macromodels via Hamiltonian-driven multivariate adaptive sampling

Alessandro Zanco, *Student Member, IEEE*, Stefano Grivet-Talocia, *Fellow, IEEE*, Tommaso Bradde, *Student Member, IEEE*, Marco De Stefano, *Student Member, IEEE*

***Abstract*—We present an algorithm for passivity verification and enforcement of multivariate macromodels whose state-space matrices depend in closed form on a set of external or design parameters. Uniform passivity throughout the parameter space is a fundamental requirement of parameterized macromodels of physically passive structures, that must be guaranteed during model generation. Otherwise, numerical instabilities may occur, due to the ability of non-passive models to generate energy.**

In this work, we propose the first available algorithm that, starting from a generic parameter-depedent state-space model, identifies the regions in the frequency-parameter space where the model behaves locally as a non-passive system. The approach we pursue is based on an adaptive sampling scheme in the parameter space, which iteratively constructs and perturbs the eigenvalue spectrum of suitable Skew-Hamiltonian/Hamiltonian (SHH) pencils, with the objective of identifying the regions where some of these eigenvalues become purely imaginary, thus pinpointing local passivity violations. The proposed scheme is able to detect all relevant violations. An outer iterative perturbation method is then applied to the model coefficients in order to remove such violations and achieve uniform passivity. Although a formal proof of global convergence is not available, the effectiveness of the proposed implementation of the passivity verification and enforcement schemes is demonstrated on several examples.

***Index Terms*—Passivity, Hamiltonian matrices, Data-driven Model Order Reduction, Scattering, Immittance, Descriptor Systems.**

I. Introduction and Motivation

This paper addresses the problem of constructing accurate and robust behavioral reduced-order models (ROM), henceforth denoted as *macromodels*, of complex dynamical systems, including explicit dependence on external parameters. Macromodels aim at reproducing with the required level of accuracy the response of a given system, but with a drastically reduced complexity in the constitutive equations, allowing for reliable simulations in a fraction of the runtime that would be required by solving the complete system using a first-principle solver.

Adoption of reduced-order models in computer-aided design flows is widespread in several application areas, ranging from microelectronics [1]–[3] to power systems [4], [5], multiphysics systems including thermal, mechanical and electrical domains [6]–[9], and many others. Although highly efficient and reliable macromodeling algorithms exist and are embedded in modern CAD tools, research in Model Order Reduction (MOR) is very active both in applied engineering fields and in mathematics, since various open problems still exist.

There are two main approaches for macromodeling, depending on the initial description of the system. Classical reduction approaches start from an internal description, usually in terms of state-space or descriptor equations, which are truncated or projected onto lower-dimensional subspaces. See [6], [10]–[14] for an overview. Conversely, data-driven approaches start from a black-box description of the system in terms of its input-output responses in time or frequency domain, and perform some interpolation or fitting of a given model structure to these data through an approximation or identification process [15]–[18]. The latter approach derives models from direct measurements or from results of numerical field simulations, e.g. from commercial field solvers, without any a priori assumption on the internal structure of the system under modeling. The main focus of this work is on the latter data-driven approach, although the proposed algorithms are general and can be applied to models obtained by any preferred MOR technique.

We consider general Linear Time-Invariant (LTI) systems, whose responses depend on a set of parameters. These may be related to geometry, material, temperature or any other variable the system responses may depend on. We assume to know sampled frequency responses over a prescribed frequency band and over the parameter space, and we want to derive parameterized macromodels in state-space form, whose responses match as closely as possible the original responses. Several algorithms are available for this task, including multivariate rational fitting [6], [19], [20], Loewner-based approaches [21], and interpolation methods [22]–[26]. We assume in particular that some initial parameterized model is already available, as resulting from one of these methods, so our starting point will be a parameter-dependent state-space (descriptor) system. The main problem that we address in this work is the verification and the enforcement of uniform passivity of this model.

A passive system is unable to generate energy on its own. This fundamental physical property must be reflected numerically in any model that intends to represent the system, since a non-passive model may result in unrealistic results during system-level simulation, including unstable behavior. Construction of passive non-parameterized models can be considered as a solved problem, thanks to many reliable algorithms, see [6], [27] for an overview. Conversely, the construction of parameterized models that are uniformly passive throughout the parameter space is stil a partially open problem. Some existing algorithms for data-driven parameterized macromodeling [19] are not able to guarantee model passivity throughout the parameter space, and this motivates our work.

Some other approaches are available that guarantee passivity by construction. These approaches usually perform an interpolation of a set of non-parameterized passive macromodels using passivity-preserving interpolation schemes. Some of these approaches [22]–[25] produce models with higher complexity than necessary. Some other approaches control both complexity and passivity but perform interpolation of state-space matrices [26], which may be questionable due to the non-unicity of state-space realizations.

Our starting point is a possibly non-passive macromodel known as a parameterized state-space (descriptor) form. We first present an algorithm that is able to verify passivity, by extending to the parametric case the class of Hamiltonian-based methods originally presented in [28] and later extended in [29]. Our framework starts from the formulation [28], where however only a single parameter was considered, and extends it to the general case of a multivariate parameter space. A second contribution involves a more general model structure, hence granting wider applicability. A further novel contribution is a new formulation of a multivariate adaptive sampling algorithm in the parameter space, based on a first-order perturbation of the eigenvalue spectrum of a suitably-defined Skew-Hamiltonian Hamiltonian (SHH) pencil, which allows to localize the passivity violations in the frequency-parameter space, and which proves much more reliable than the method based on the spectral abscissa presented in [28]. Once the passivity violations are detected, an iterative perturbation scheme is presented that is able to remove them by minimizing model error while enforcing local passivity constraints. This paper presents the complete framework and extends some preliminary results presented in [30].

II. Preliminaries and Notation

We consider a general descriptor (non-impulsive) system with a square $P \times P$ transfer matrix

$$\mathbf{H}(s,\boldsymbol{\vartheta}) = \mathbf{C}(\boldsymbol{\vartheta})\left(s\mathbf{E} - \mathbf{A}(\boldsymbol{\vartheta})\right)^{-1}\mathbf{B} \tag{1}$$

with real realization matrices $\mathbf{E}, \mathbf{A} \in \mathbb{R}^{\bar{N}\times\bar{N}}$, $\mathbf{B} \in \mathbb{R}^{\bar{N}\times P}$ and $\mathbf{C} \in \mathbb{R}^{P\times\bar{N}}$. In addition to complex frequency s, the transfer matrix depends on a set of external parameters, collected in vector $\boldsymbol{\vartheta} \in \Theta \subseteq \mathbb{R}^{\rho}$. The parameter space is here assumed to be a ρ-dimensional box, whose edges along the ν-th dimension are $[\vartheta^{\nu}_{\min}, \vartheta^{\nu}_{\max}]$. Without loss of generality, we will assume in the following a normalized hypercube with $\vartheta^{\nu}_{\min} = 0$ and $\vartheta^{\nu}_{\max} = 1$.

As typical in most applications, the system parameterization in (1) assumes a constant input-state map $\mathbf{B}$ and a constant descriptor matrix $\mathbf{E}$. The latter assumption is not essential and can be released, as far as the pencil $(\mathbf{A}(\boldsymbol{\vartheta}), \mathbf{E})$ is regular[1] $\forall\boldsymbol{\vartheta} \in \Theta$. This condition ensures that the transfer matrix $\mathbf{H}(s,\boldsymbol{\vartheta})$ is well-defined throughout the frequency and parameter ranges. There is no additional restriction on $\mathbf{E}$, which may be singular.

[1] a pencil $(\mathbf{A}, \mathbf{E})$ is *regular* if $\exists s \in \mathbb{C}$ such that $|s\mathbf{E} - \mathbf{A}| \neq 0$.

The specific parameterization scheme that we consider in this work is based on the following linear expansions

$$\mathbf{A}(\boldsymbol{\vartheta}) = \sum_{\ell=1}^{\bar{\ell}} \mathbf{A}_\ell\, \xi_\ell(\boldsymbol{\vartheta}), \quad \mathbf{C}(\boldsymbol{\vartheta}) = \sum_{\ell=1}^{\bar{\ell}} \mathbf{C}_\ell\, \xi_\ell(\boldsymbol{\vartheta}) \tag{2}$$

of the two parameter-dependent matrices into a set of multivariate basis functions $\xi_\ell(\boldsymbol{\vartheta})$ with constant coefficients $\mathbf{A}_\ell, \mathbf{C}_\ell$, where $\ell = 1, \ldots, \bar{\ell}$ denotes a global linear index that spans the adopted multivariate basis. The above parameterization generalizes in several aspects the expected transfer function dependence of arbitrary RLC lumped circuits, when viewed as functions of frequency and individual circuit parameters. It is well-known that any such transfer function is a rational function of complex frequency s,

$$\mathbf{H}(s;\boldsymbol{\vartheta}) = \frac{\mathbf{N}(s,\boldsymbol{\vartheta})}{\mathsf{D}(s,\boldsymbol{\vartheta})} = \frac{\sum_{n=0}^{\bar{n}} \mathbf{R}_n(\boldsymbol{\vartheta})\,\varphi_n(s)}{\sum_{n=0}^{\bar{n}} r_n(\boldsymbol{\vartheta})\,\varphi_n(s)}, \tag{3}$$

with coefficients $\mathbf{R}_n(\boldsymbol{\vartheta}), r_n(\boldsymbol{\vartheta})$ that are multiaffine in the circuit parameters $\boldsymbol{\vartheta}$, with $\varphi_n(s) = s^n$. We preserve the rational form of (3) as a function of s, so that our model corresponds to a finite-order Ordinary Differential Equation (ODE) system in time-domain, but we replace the monomials s^n with the partial fraction basis $\varphi_0(s) = 1$ and $\varphi_n(s) = (s - q_n)^{-1}$ for $n > 0$, where q_n are predefined stable "basis poles", in order to improve numerical conditioning in the initial model extraction phase. Then, we extend the multi-affine dependence of the coefficients to higher-order polynomials, in order to allow for general parameters (not only circuit element values) and to extend applicability to more general electromagnetic structures, and not necessarily lumped circuits. The resulting model structure is equivalent to a parameterized barycentric form, which is a standard [6], [8], [15], [16]. The assumed descriptor form (1) is easily derived from (3), see e.g. [19], in which case the state-space size is obtained as $\bar{N} = (\bar{n}+1)P$. We remark that the above structure implicitly parameterizes the model poles (which may have non-smooth trajectories in the parameter space) through smoothly varying numerator and denominator coefficients. The identification of the model coefficients from frequency response data is textbook material and is not repeated here, see [6] and also [29], [31].

In this work, we will consider each basis function $\xi_\ell(\boldsymbol{\vartheta})$ in (2) to be the product of univariate basis functions

$$\xi_\ell(\boldsymbol{\vartheta}) = \xi_{\ell_1}(\vartheta^1) \cdot \xi_{\ell_2}(\vartheta^2) \cdots \xi_{\ell_\rho}(\vartheta^\rho) \tag{4}$$

where a suitable mapping between global index ℓ and the multi-index $(\ell_1, \ell_2, \ldots, \ell_\rho)$ is established. In particular, all numerical examples in this work are based on (first kind) Chebychev polynomials along each direction in the parameter space, so that $\xi_{\ell_\nu}(\vartheta^\nu)$ is the Chebychev polynomial defined on interval $[\vartheta^{\nu}_{\min}, \vartheta^{\nu}_{\max}]$ with degree ℓ_ν, up to a maximum degree $\bar{\ell}_\nu$. This results in $(1 + \bar{\ell}_\nu)$ univariate basis functions along each direction ν, which results in a cardinality $\bar{\ell}$ of the global index ℓ expressed by the product

$$\bar{\ell} = \prod_{\nu=1}^{\rho} (1 + \bar{\ell}_\nu). \tag{5}$$

We remark that this choice of basis functions is not restrictive, as any structured/nonstructured bases can be used to expand $\mathbf{A}(\boldsymbol{\vartheta})$ and $\mathbf{C}(\boldsymbol{\vartheta})$ through (2). Chebychev polynomials have been chosen here for their good numerical properties. However, as proposed in [20] where the Fourier basis was used to handle a periodically-varying dependence, other bases can be chosen according to the problem at hand. For our purposes, $\xi_\ell(\boldsymbol{\vartheta})$ must be differentiable throughout Θ.

An important requirement that we will assume in the following is the uniform asymptotic stability of $\mathbf{H}(s,\boldsymbol{\vartheta})$, which implies that all finite eigenvalues of pencil $(\mathbf{A}(\boldsymbol{\vartheta}),\mathbf{E})$ have a strictly negative real part $\forall\boldsymbol{\vartheta}\in\Theta$. Using the constrained Parameterized Sanathanan-Koerner (PSK) algorithm outlined in [29] to construct the model, the above assumptions on both model structure and uniform stability are verified by construction.

Some remarks on the adopted notation are in order. We denote scalars with lowercase italic fonts x, vectors with lowercase bold fonts $\mathbf{x}$, and matrices with uppercase bold fonts $\mathbf{X}$. Throughout this paper, * denotes the complex conjugate; $\mathbf{X}^\mathsf{T}$ and $\mathbf{X}^\mathsf{H}$ are the transpose and hermitian transpose of matrix $\mathbf{X}$, respectively. A positive semi-definite symmetric (or hermitian symmetric) matrix is denoted as $\mathbf{X}\geq 0$. We generally denote the upper limit of some index ℓ through an overbar, as $\bar{\ell}$. The spectrum of eigenvalues and singular values of $\mathbf{X}$ are denoted as $\lambda(\mathbf{X})$ and $\sigma(\mathbf{X})$, respectively.

III. Passivity conditions

The conditions that characterize a passive transfer matrix $\mathbf{H}(s,\boldsymbol{\vartheta})$ depend on its particular input-output representation [32], [33]. Here we consider the two most common cases of immittance (including impedance, admittance or hybrid) and scattering representations. The following two conditions must hold in all cases

a) $\mathbf{H}(s,\boldsymbol{\vartheta})$ is regular for $\Re\{s\}>0$ and $\forall\boldsymbol{\vartheta}\in\Theta$,
b) $\mathbf{H}^*(s,\boldsymbol{\vartheta})=\mathbf{H}(s^*,\boldsymbol{\vartheta})$, $\forall s\in\mathbb{C}$ and $\forall\boldsymbol{\vartheta}\in\Theta$,

Condition a) is related to the uniform model stability, which is here assumed a priori, whereas b) implies a real impulse response and is here guaranteed by the real-valued descriptor realization.

Passivity is fully characterized by an additional dissipation condition, which ensures that the system is unable to generate energy. The particular form of this condition depends on the system representation

A. Immittance representations

In the immittance case, a passive transfer matrix must be *Positive-Real* (PR). In our parameterized setting, PR-ness will be required to hold uniformly in the parameter space $\forall\boldsymbol{\vartheta}\in\Theta$ through

c) $\boldsymbol{\Psi}_I(s,\boldsymbol{\vartheta})=\mathbf{H}(s,\boldsymbol{\vartheta})+\mathbf{H}^\mathsf{H}(s,\boldsymbol{\vartheta})\geq 0$ for $\Re\{s\}>0$.

Given our working assumptions, a simpler but equivalent form for this condition can be stated as

$$\lambda_{\min}(\mathbf{H}(\mathrm{j}\omega,\boldsymbol{\vartheta})+\mathbf{H}^\mathsf{H}(\mathrm{j}\omega,\boldsymbol{\vartheta}))\geq 0\quad\forall\omega\in\mathbb{R},\forall\boldsymbol{\vartheta}\in\Theta \tag{6}$$

where $\lambda_{\min}(\cdot)$ denotes the smallest eigenvalue of its matrix argument. It is sufficient to check this minimum eigenvalue for $s=\mathrm{j}\omega$ thanks to the assumed uniform asymptotic stability, which guarantees that the transter matrix $\mathbf{H}(s,\boldsymbol{\vartheta})$ is regular when restricted to the imaginary axis.

B. Scattering representations

In the scattering case, a passive transfer matrix must be *Bounded-Real* (BR). This condition is expressed in our parameterized setting $\forall\boldsymbol{\vartheta}\in\Theta$ as

d) $\boldsymbol{\Psi}_S(s,\boldsymbol{\vartheta})=\mathbf{I}-\mathbf{H}^\mathsf{H}(s,\boldsymbol{\vartheta})\mathbf{H}(s,\boldsymbol{\vartheta})\geq 0$ for $\Re\{s\}>0$

Also in this case a simpler equivalent form is available as

$$\lambda_{\min}(\mathbf{I}-\mathbf{H}^\mathsf{H}(\mathrm{j}\omega,\boldsymbol{\vartheta})\mathbf{H}(\mathrm{j}\omega,\boldsymbol{\vartheta}))\geq 0\quad\forall\omega\in\mathbb{R},\forall\boldsymbol{\vartheta}\in\Theta \tag{7}$$

or, equivalently,

$$\sigma_{\max}(\mathbf{H}(\mathrm{j}\omega,\boldsymbol{\vartheta}))\leq 1\quad\forall\omega\in\mathbb{R},\forall\boldsymbol{\vartheta}\in\Theta \tag{8}$$

where $\sigma_{\max}(\cdot)$ denotes the largest singular value of its matrix argument.

IV. Problem statement

The main objective of this work is enforcing uniform passivity of a given parameterized model in form (1). This operation requires two main steps, discussed below.

A. Passivity check

This step involves a localization and a quantification of any passivity violations. This is achieved by finding the regions $\Theta_\alpha\subset\Theta$ for $\alpha=1,2,\dots$ where conditions (6) or (8) do not hold. Within each such region, we are interested in the worst-case local passivity violation extent, defined as

$$\bar{\lambda}^\alpha_{\min}=\inf_{\omega\in\mathbb{R},\boldsymbol{\vartheta}\in\Theta_\alpha}\lambda_{\min}(\mathbf{H}(\mathrm{j}\omega,\boldsymbol{\vartheta})+\mathbf{H}^\mathsf{H}(\mathrm{j}\omega,\boldsymbol{\vartheta})) \tag{9}$$

for immittance systems and

$$\bar{\sigma}^\alpha_{\max}=\sup_{\omega\in\mathbb{R},\boldsymbol{\vartheta}\in\Theta_\alpha}\sigma_{\max}(\mathbf{H}(\mathrm{j}\omega,\boldsymbol{\vartheta})) \tag{10}$$

for scattering systems, together with their localization $(\bar{\omega}_\alpha,\bar{\boldsymbol{\vartheta}}_\alpha)$ in the frequency-parameter space. Since these denote local passivity violations, we have $\bar{\lambda}^\alpha_{\min}<0$ and $\bar{\sigma}^\alpha_{\max}>1$. Our approach to this passivity check is addressed in detail in Sec. VI.

B. Passivity enforcement

This step formulates a perturbation scheme that corrects the realization matrices by enforcing passivity constraints. These constraints are best defined based on the information on the passivity violations collected during the check, expressed by the triplets $\{\bar{\omega}_\mu,\bar{\boldsymbol{\vartheta}}_\mu;\bar{\lambda}^\mu_{\min}\}$ in the immittance case and $\{\bar{\omega}_\mu,\bar{\boldsymbol{\vartheta}}_\mu;\bar{\sigma}^\mu_{\max}\}$ in the scattering case. In the following, these sets will be denoted by the common notation $\mathcal{W}_\mu$ for both representations, with $\mathcal{W}=\{\mathcal{W}_\mu,\ \mu=1,2,\dots\}$.

Our proposed perturbation scheme will iteratively correct an initially non-passive model by enforcing approximate passivity constraints at each iteration, thus requiring repeated passivity checks for setting up these constraints. The iterations will stop when $\mathcal{W}$ becomes empty. The main passivity enforcement scheme is described in Sec. VII.

V. Hamiltonian-Based Passivity Characterization

Both proposed passivity check and enforcement algorithms are based on the spectral properties of some Skew-Hamiltonian/Hamiltonian (SHH) pencils associated to (1), which are reviewed below [6], [34]–[36]. For immittance representations, we define the SHH pencil $(\mathbf{M}_I(\boldsymbol{\vartheta}), \mathbf{K}_I)$ as

$$\mathbf{M}_I(\boldsymbol{\vartheta}) = \begin{pmatrix} \mathbf{A}(\boldsymbol{\vartheta}) & \mathbf{0} & \mathbf{B} \\ \mathbf{0} & -\mathbf{A}^{\mathsf{T}}(\boldsymbol{\vartheta}) & -\mathbf{C}^{\mathsf{T}}(\boldsymbol{\vartheta}) \\ \mathbf{C}(\boldsymbol{\vartheta}) & \mathbf{B}^{\mathsf{T}} & \mathbf{0} \end{pmatrix} \qquad (11)$$

$$\mathbf{K}_I = \begin{pmatrix} \mathbf{E} & \mathbf{0} & \mathbf{0} \\ \mathbf{0} & \mathbf{E}^{\mathsf{T}} & \mathbf{0} \\ \mathbf{0} & \mathbf{0} & \mathbf{0} \end{pmatrix}$$

while for scattering models we define the SHH pencil $(\mathbf{M}_S(\boldsymbol{\vartheta}), \mathbf{K}_S)$ as

$$\mathbf{M}_S(\boldsymbol{\vartheta}) = \begin{pmatrix} \mathbf{A}(\boldsymbol{\vartheta}) & \mathbf{B}\mathbf{B}^{\mathsf{T}} \\ -\mathbf{C}^{\mathsf{T}}(\boldsymbol{\vartheta})\mathbf{C}(\boldsymbol{\vartheta}) & -\mathbf{A}^{\mathsf{T}}(\boldsymbol{\vartheta}) \end{pmatrix} \qquad (12)$$

$$\mathbf{K}_S = \begin{pmatrix} \mathbf{E}^{\mathsf{T}} & \mathbf{0} \\ \mathbf{0} & \mathbf{E} \end{pmatrix}.$$

The following theorems (see [37] and [6, Chapter 9]) hold for the two representations, respectively.

Theorem 1: Let the matrix pencil $(\mathbf{A}(\boldsymbol{\vartheta}), \mathbf{E})$ have no purely imaginary eigenvalues. Then, $\mathrm{j}\omega_i$ is a generalized eigenvalue of $(\mathbf{M}_I(\boldsymbol{\vartheta}), \mathbf{K}_I)$ if and only if $\lambda = 0$ is an eigenvalue of $\boldsymbol{\Psi}_I(\mathrm{j}\omega_i, \boldsymbol{\vartheta})$.

Theorem 2: Let the matrix pencil $(\mathbf{A}(\boldsymbol{\vartheta}), \mathbf{E})$ have no purely imaginary eigenvalues. Then, $\mathrm{j}\omega_i$ is a generalized eigenvalue of $(\mathbf{M}_S(\boldsymbol{\vartheta}), \mathbf{K}_S)$ if and only if $\lambda = 0$ is an eigenvalue of $\boldsymbol{\Psi}_S(\mathrm{j}\omega_i, \boldsymbol{\vartheta})$ or, equivalently, $\sigma = 1$ is a singular value of $\mathbf{H}(\mathrm{j}\omega_i, \boldsymbol{\vartheta})$.

Assuming the parameters to be fixed to some nominal value $\boldsymbol{\vartheta} = \boldsymbol{\vartheta}_q$, the above results can be exploited to localize all passivity violations of the corresponding model $\mathbf{H}(s, \boldsymbol{\vartheta}_q)$ through a purely algebraic test. The purely imaginary eigenvalues $\mathrm{j}\omega_i$ of the appropriate SHH pencil are first computed. At the corresponding frequencies ω_i, one eigenvalue of $\boldsymbol{\Psi}_I(\mathrm{j}\omega, \boldsymbol{\vartheta}_q)$ or $\boldsymbol{\Psi}_S(\mathrm{j}\omega, \boldsymbol{\vartheta}_q)$ changes sign[2]. Therefore, these frequencies subdivide the frequency axis into disjoint subbands which are locally passive or locally non-passive. A local eigenvalue sampling in each non-passive subband can thus be used to determine the worst-case passivity violations $\mathcal{W}_q$. This characterization for fixed $\boldsymbol{\vartheta} = \boldsymbol{\vartheta}_q$ is illustrated in Fig. 1. We remark that the above procedure is standard and is generally considered as the method of choice for passivity check of non-parameterized models.

Let us now consider the model behavior for a parameter configuration that deviates from the above nominal value as $\boldsymbol{\vartheta} = \boldsymbol{\vartheta}_q + \delta\boldsymbol{\vartheta}$. Correspondingly, the SHH pencil is modified, as well as its eigenspectrum. Figure 2 illustrates the trajectories that the SHH eigenvalues follow (blue dotted lines) starting from a nominal parameter configuration (yellow dots). It may happen that some non-imaginary eigenvalues become purely imaginary (thus inducing new passivity violation bands), and vice-versa. Therefore, the characterization of all passivity violations is inevitably parameter-dependent and requires a multivariate extension of the standard Hamiltonian check to the entire parameter space. This is investigated next.

[2]we avoid here technical conditions on Hamiltonian eigenvalue multiplicity by assuming simple eigenvalues only, see [38] for a complete discussion.

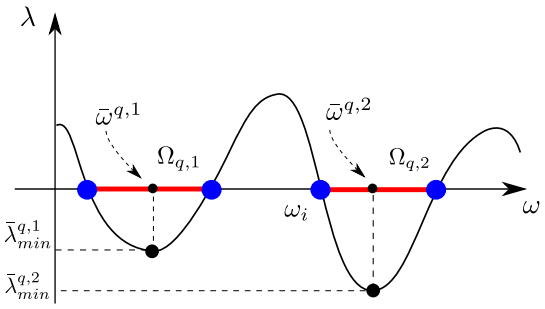

Fig. 1: Representation of one eigenvalue of $\boldsymbol{\Psi}_I(\mathrm{j}\omega, \boldsymbol{\vartheta}_q)$ corresponding to a fixed parameter value $\boldsymbol{\vartheta}_q$. The eigenvalue λ (solid black line) crosses the zero baseline for $\omega = \omega_i$ (the imaginary SHH eigenvalues, blue large dots), delimiting non-passive frequency bands $\Omega_{q,1}$, $\Omega_{q,2}$ (highlighted as thick red lines). Local minima are denoted as small black dots.

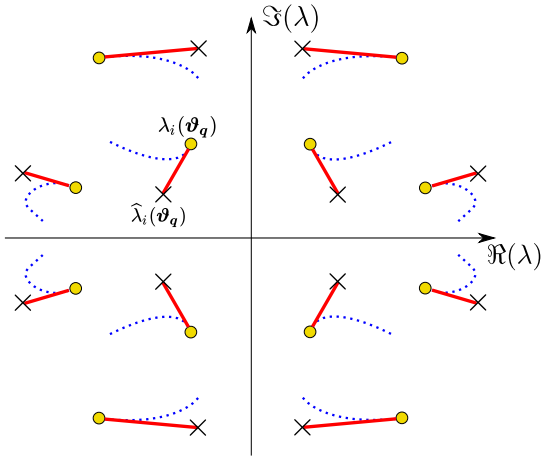

Fig. 2: First-order approximation (red solid lines) of SHH eigenvalue trajectories (blue dotted lines) along a one-dimensional path in the parameter space. Circles denote the nominal eigenvalues, while crosses are the first-order eigenvalue estimates.

VI. Predictive Passivity Verification via SHH Pencil Perturbation

The main approach that we follow for multivariate (parameterized) passivity verification is based on an adaptive sampling process in the parameter space Θ. This process is summarized as follows.

1) We start from an initial distribution of parameter values $\boldsymbol{\vartheta}_q$ for $q = 1, \ldots, \bar{q}$;
2) we determine the finite SHH spectra Λ_q at each available parameter value $\boldsymbol{\vartheta}_q$;
3) based on the above spectra, we determine whether the available samples $\boldsymbol{\vartheta}_q$ are sufficient to completely characterize all passivity violations $\forall \boldsymbol{\vartheta} \in \Theta$, or whether some refinement in the sampling density is needed in some regions;

4) in case a refined sampling is required, new $\Delta\bar{q}$ samples are added. The process is repeated from step 2) until no new samples are required or a maximum number of iterations is reached. We denote these as "inner" iterations.

The above procedure may seem straightforward, but it is in fact quite challenging: we need to infer that some passivity violations exist (or do not exist) in a continuous parameter space Θ, based only on a finite number of "measurement" points $\boldsymbol{\vartheta}_q$. Therefore, the verification method must be equipped with some prediction capability that is able to provide information on passivity violations in a neighborhood of each point $\boldsymbol{\vartheta}_q$, and not only exactly at $\boldsymbol{\vartheta}_q$. This information is sought for in form of presence (or guaranteed absence) of purely imaginary SHH eigenvalues.

A. Notation

We first introduce a compact notation that will prove useful in the following. Consider a matrix-valued function $\mathbf{X}(\boldsymbol{\vartheta}) \in \mathbb{R}^{m,n}$, where $\boldsymbol{\vartheta} \in \mathbb{R}^{\rho}$. We collect the first-order partial derivatives with respect to $\boldsymbol{\vartheta}$ in a 3-way tensor, denoted as $\mathcal{D}\{\mathbf{X}(\boldsymbol{\vartheta})\} \in \mathbb{R}^{m,n,\rho}$, where

$$\mathcal{D}\{\mathbf{X}(\boldsymbol{\vartheta})\}_{i,j,\nu} = \frac{\partial X_{i,j}(\boldsymbol{\vartheta})}{\partial \vartheta^{\nu}}. \tag{13}$$

Evaluation of the partial derivative tensor at $\boldsymbol{\vartheta}_q$ will be denoted as $\mathcal{D}_{\boldsymbol{\vartheta}_q}\{\mathbf{X}(\boldsymbol{\vartheta})\}$.

A first-order Taylor expansion of matrix element $X_{i,j}(\boldsymbol{\vartheta})$ centered at $\boldsymbol{\vartheta}_q$ reads

$$X_{i,j}(\boldsymbol{\vartheta}_q + \delta\boldsymbol{\vartheta}) \approx X_{i,j}(\boldsymbol{\vartheta}_q) + \nabla_{\boldsymbol{\vartheta}_q} X_{i,j}(\boldsymbol{\vartheta})^{\mathsf{T}} \cdot \delta\boldsymbol{\vartheta} \tag{14}$$

where ∇ denotes the gradient operator, which can be written for the entire matrix $\mathbf{X}(\boldsymbol{\vartheta})$ through the compact notation

$$\mathbf{X}(\boldsymbol{\vartheta}_q + \delta\boldsymbol{\vartheta}) \approx \mathbf{X}(\boldsymbol{\vartheta}_q) + \mathcal{D}_{\boldsymbol{\vartheta}_q}\{\mathbf{X}(\boldsymbol{\vartheta})\} \times_3 \delta\boldsymbol{\vartheta} \tag{15}$$

where the operator $\times_r$ denotes the r-mode tensor product [39].

B. Differentiating SHH pencils and SHH eigenvalues

Let us consider the descriptor realization matrices defined in Sec. II. The derivative tensors associated to $\mathbf{A}(\boldsymbol{\vartheta}), \mathbf{C}(\boldsymbol{\vartheta})$ can be evaluated in closed form, since their parameter dependence is induced by the known basis functions $\xi_{\ell}(\boldsymbol{\vartheta})$. We have

$$\mathcal{D}\{\mathbf{A}(\boldsymbol{\vartheta})\} = \sum_{\ell=1}^{\bar{\ell}} \mathbf{A}_{\ell} \circ \nabla\xi_{\ell}(\boldsymbol{\vartheta}), \tag{16}$$

and similarly for $\mathbf{C}(\boldsymbol{\vartheta})$, where $\circ$ denotes the outer product [39]. Based on these expressions, we can construct the derivative tensors of the SHH pencils through simple algebraic manipulations (omitted). For both immittance and scattering representations (we therefore omit subscripts $_{I,S}$), we can then write the following first-order perturbation

$$\mathbf{M}(\boldsymbol{\vartheta}_q + \delta\boldsymbol{\vartheta}) \approx \mathbf{M}(\boldsymbol{\vartheta}_q) + \mathcal{D}_{\boldsymbol{\vartheta}_q}\{\mathbf{M}(\boldsymbol{\vartheta})\} \times_3 \delta\boldsymbol{\vartheta}. \tag{17}$$

Let us now consider a finite eigenvalue $\lambda_i(\boldsymbol{\vartheta}_q)$ of the pencil $(\mathbf{M}(\boldsymbol{\vartheta}_q), \mathbf{K})$ centered at some prescribed point $\boldsymbol{\vartheta}_q$ in the parameter space, and let us denote with $\mathbf{u}_i, \mathbf{v}_i$ its associated right and left eigenvectors. Using standard eigenvalue perturbation theory results [38], [40], we can estimate the trajectory of this eigenvalue along the path $\boldsymbol{\vartheta} = \boldsymbol{\vartheta}_q + \delta\boldsymbol{\vartheta}$ as

$$\widehat{\lambda}_i(\boldsymbol{\vartheta}) \approx \lambda_i(\boldsymbol{\vartheta}_q) + \delta\lambda_i(\boldsymbol{\vartheta}_q), \tag{18}$$

where the first-order perturbation term reads

$$\delta\lambda_i(\boldsymbol{\vartheta}_q) \approx \frac{\mathcal{D}_{\boldsymbol{\vartheta}_q}\{\mathbf{M}(\boldsymbol{\vartheta})\} \times_1 \mathbf{v}_i^* \times_2 \mathbf{u}_i \times_3 \delta\boldsymbol{\vartheta}}{\mathbf{v}_i^{\mathsf{H}} \cdot \mathbf{K} \cdot \mathbf{u}_i} \tag{19}$$

We remark that the above tensor notation does not lead to computational advantages but rather allows for a more clear definition of the various operations to be performed, as well as to a cleaner coding.

Figure 2 depicts the above eigenvalue perturbation results on an illustrative case. The yellow dots represent the nominal finite SHH eigenvalues $\{\lambda_i(\boldsymbol{\vartheta}_q)\}$, the blue dotted lines denote the exact trajectories $\{\lambda_i(\boldsymbol{\vartheta}_q + \delta\boldsymbol{\vartheta})\}$ on a one-dimensional cut $\delta\boldsymbol{\vartheta} = \mathbf{p}\,\delta t$ along some direction $\mathbf{p} \in \mathbb{R}^{\rho}$ with $\|\mathbf{p}\| = 1$; the red solid lines represent the linearization of these trajectories, leading to the linear predictions (crosses) based on (18)–(19). As expected, the linear predictions are only valid for small δt and are tangent to the exact trajectories for $\delta t = 0$.

C. Adaptive sampling via SHH spectral perturbation

The above derivation showed that a linear perturbation analysis allows to predict the location of all SHH eigenvalues in a neighborhood of a given expansion point $\boldsymbol{\vartheta}_q$. We now exploit this capability to set up an adaptive sampling scheme for the localization of passivity violations in the parameter space Θ. To this end, we consider a dynamically and adaptively constructed partition. We proceed in steps.

1) Initialization: We first subdivide each parameter space direction $\nu = 1, \ldots, \rho$ into $2^{j_0^{\nu}}$ identical sub-intervals, with j_0^{ν} the initial refinement level, whose end points are collected in set $\mathcal{S}_{j_0^{\nu}} = \{k\,2^{-j_0^{\nu}},\ k = 0, \ldots, 2^{j_0^{\nu}}\}$. The Cartesian product:

$$\mathcal{V}_0 = \mathcal{S}_{j_0^1} \times \mathcal{S}_{j_0^2} \times, \ldots, \times \mathcal{S}_{j_0^{\rho}} \tag{20}$$

defines the set of vertices $\boldsymbol{\vartheta}_q \in \mathcal{V}_0$, identified by a global index $q = 1, \ldots, \bar{q}$, of a (hyper)-cubic lattice providing an initial uniform partition of Θ (see top-left panel of Fig. 5 for a 2D example with $\rho = 2$). This partition is described through a data structure $\mathcal{P}_0 = \{\mathcal{V}_0, \mathcal{E}_0, \mathcal{F}_0\}$, where edges connecting any pair of adjacent vertices are collected in set $\mathcal{E}_0$, and all (hyper)-cubic cells Γ_{τ} for $\tau = 1, \ldots, \bar{\tau}$ are collected in set $\mathcal{F}_0$.

Then, we extract and store all the (finite) SHH eigenvalues $\lambda_{q,i} = \lambda_i(\boldsymbol{\vartheta}_q) \in \Lambda_q$ with associated left and right eigenvectors. Note that only the eigenvalues in any closed quadrant (we consider the second quadrant in the following) are sufficient, due to the four-quadrant symmetry of the SHH spectrum. The frequencies $\omega_{q,i}$ corresponding to the purely imaginary eigenvalues $\lambda_{q,i} = \mathrm{j}\omega_{q,i}$ are sorted in ascending order and collected in a set Ω_q. If $\Omega_q = \emptyset$, then $\boldsymbol{\vartheta}_q$ is labelled as "passive" (green empty dots in Fig. 5) based on Theorems 1-2. Otherwise $\boldsymbol{\vartheta}_q$ corresponds to a non-passive vertex (red filled dots in Fig. 5). With reference to Fig. 1, we perform a local fine frequency sampling on each non-passive

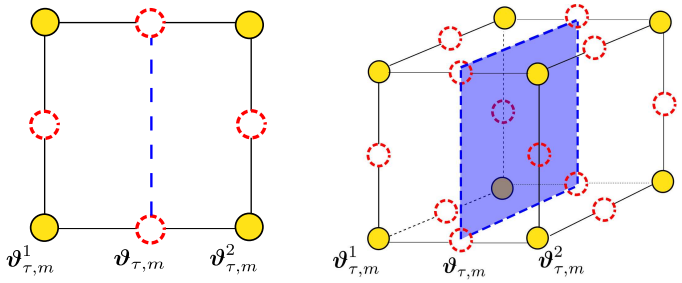

(a) $\rho = 2$ (b) $\rho = 3$

Fig. 3: Elementary cell Γ_τ in 2D (left) and 3D (right) being refined along the first direction $\nu = 1$. Filled yellow dots and red dashed dots represent vertices and edge midpoints, respectively.

band $\Omega_{q,\beta}$ (highlighted in red) for $\beta = 1, \ldots, \bar{\beta}_q$ to detect the worst-case passivity violations, occurring at frequencies $\bar{\omega}_\mu = \bar{\omega}^{q,\beta}$. These will be collectively identified as $\mathcal{W}_\mu$, with μ a unique index whose upper bound $\bar{\mu}$ is increased anytime a new violation is added.

2) Grid refinement: We consider grid refinement starting from a generic refinement iteration $J = 0, 1, \ldots$, where $J = 0$ corresponds to the above initialization. We process all cells $\Gamma_\tau \in \mathcal{F}_J$ in a loop for $\tau = 1, \ldots, \bar{\tau}$. For each current cell Γ_τ (see Fig. 3) we extract all support edges $\mathbf{e}_{\tau,m} \in \mathcal{E}_J$ for $m = 1, \ldots, \rho\, 2^{\rho-1}$, we calculate the coordinates of the corresponding midpoints $\boldsymbol{\vartheta}_{\tau,m}$ (dashed red dots), and we denote the two local vertices at their endpoints as $\boldsymbol{\vartheta}^v_{\tau,m} \in \mathcal{V}_J$ for $v = 1, 2$ (yellow dots).

Since all SHH eigenvalues and eigenvectors at all vertices are available from previous iterations, we calculate the two first-order predictions $\widehat{\lambda}^v_{\tau,m;i}$ of each SHH eigenvalue at the midpoint $\boldsymbol{\vartheta}_{\tau,m}$ of each edge $\mathbf{e}_{\tau,m}$, starting from the reference eigenvalues $\lambda^v_{\tau,m;i}$ at the two endpoints $\boldsymbol{\vartheta}^v_{\tau,m}$. Based on these estimates, we add $\boldsymbol{\vartheta}_{\tau,m}$ as a new vertex if

- $\Re\{\widehat{\lambda}^v_{\tau,m;i} - \lambda^v_{\tau,m;i}\} > 0$ for some v, implying that the eigenvalue is moving closer to the imaginary axis, and at the same time
- $\Re\{\widehat{\lambda}^v_{\tau,m;i}\} > -\varepsilon$ for the same v fulfilling above condition, where $\varepsilon > 0$ is a small threshold.

Three significant cases are illustrated in Fig. 4. Case 1 (top eigenvalue) verifies both above conditions and will trigger edge refinement. Cases 2 and 3 will not trigger edge refinement since the linear eigenvalue predictions are sufficiently far from the imaginary axis.

When a midpoint $\boldsymbol{\vartheta}_{\tau,m}$ is added, also all other edge midpoints that complete the set of $2^{\rho-1}$ vertices of the $(\rho-1)$-dimensional hyperrectangle that partitions current cell Γ_τ into two equal subcells are added to construct the vertex set $\mathcal{V}_{J+1}$ for next iteration (see Fig. 3). Anytime a new vertex is added, all SHH eigenvalues and eigenvectors are precomputed and stored. Then, if the vertex is labelled as non-passive, all worst-case violations are detected and added to the set $\mathcal{W}$.

In order to save computation time, the above linear predictions are not performed

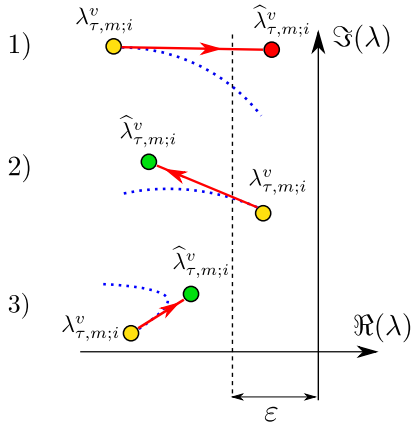

Fig. 4: Graphical representation of the adaptive refinement rules. Yellow dots: SHH eigenvalues $\lambda^v_{\tau,m;i}$ computed at vertex $\boldsymbol{\vartheta}^v_{\tau,m}$; green and red dots: linear prediction (red thick lines with arrows) of perturbed eigenvalues $\widehat{\lambda}^v_{\tau,m;i}$ at the edge midpoint $\boldsymbol{\vartheta}_{\tau,m}$; blue dotted lines: exact eigenvalue trajectories along the edge $\mathbf{e}_{\tau,m}$.

- if both edge endpoints are non-passive (in such case local passivity violations have already been detected at these endpoints and an additional refinement is not necessary);
- if one of the two endpoints is passive and the other is non-passive (in which case the midpoint is added without any further check, in order to track more precisely the boundary of the passivity violation region that inevitably occurs between these two points;
- if the reference cell Γ_τ was not refined at some previous iteration: such cells are flagged and will not be checked at any subsequent iterations.

Figure 5 shows[3] that, as the number of refinements increases, the boundaries of the passivity violation areas become better and better resolved, and even violations with a small footprint in the parameter space are detected.

The above-described adaptive subgridding scheme guarantees the subdivision of the parameter space Θ into elementary hyper-rectangular cells through iterative binary subdivision along selected directions. In order to provide a safe termination of the iterative process in case of locally nearly lossless systems, characterized by SHH eigenvalues that are uniformly very close to the imaginary axis in some parameter space regions, we stop refining when a maximum number of iterations $J_{\max}$ is reached. It is therefore possible that marginal passivity violations are missed, although this case was never observed in our tests. In any case, setting $J_{\max}$ to a sufficiently large value ensures that any undetected passivity violation has no practical importance. In our experiments we set $J_{\max}$ in the range 5–10, following the guideline of using a larger $J_{\max}$ (corresponding to more refinements) for larger parameter orders. Choosing a larger or smaller $J_{\max}$ is a tradeoff between resolution in

[3]For this illustrative example we demonstrate the passivity characterization on a linearized buffer model parameterized by supply voltage and temperature. This device is known to be locally active and locally passive in different parameter space regions, which we want to characterize.

tracking the boundaries between passive/non-passive regions and computational cost.

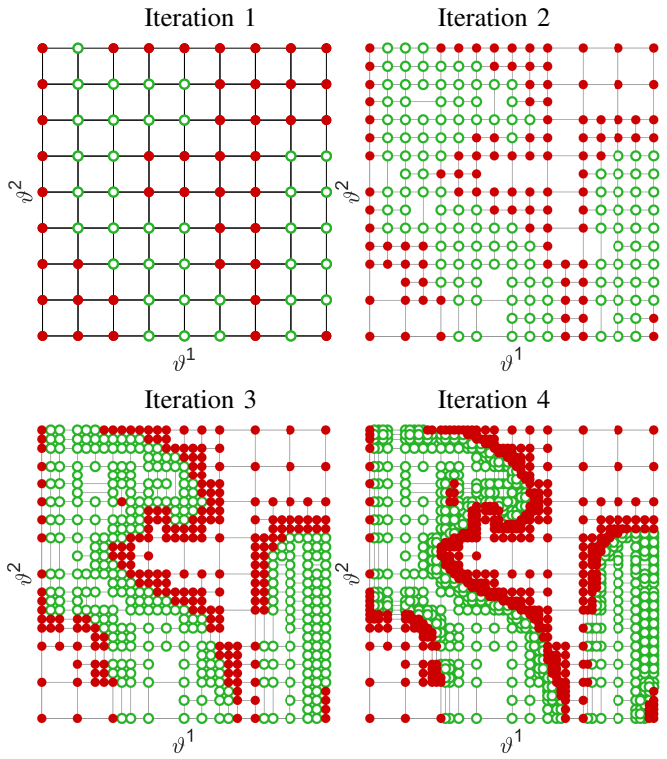

Fig. 5: Successive adaptive refinement (inner) iterations ($\rho = 2$) for the detection of passivity violation regions Θ_α of a linearized buffer model. Locally passive and non-passive regions are depicted by empty green and filled red dots, respectively.

D. Comparison with existing approaches

The proposed eigenvalue perturbation approach provides two major improvements with respect to the preliminary work in [28]. First, we extend applicability to multivariate parameter spaces, whereas [28] is limited only to one parameter $\rho = 1$. Second, grid refinement based on full-spectrum SHH perturbation proves to be much more robust with respect to the adaptive sampling of [28], where the basis for grid refinement was a bisection process on the the normalized Hamiltonian spectral distance from the imaginary axis

$$\psi(\vartheta) = \min_{\lambda(\vartheta)\in\Lambda(\vartheta)} \frac{|\,\Re\{\lambda(\vartheta)\}|}{\varrho(\vartheta)} \tag{21}$$

where $\varrho(\vartheta)$ is the spectral radius of the SHH pencil and $\Lambda(\vartheta)$ its finite eigenspectrum. Such function $\psi(\vartheta)$ is easily proved to be non-smooth, being computed as a minimum real part among all eigenvalue trajectories. This fact was already noted (see Fig. 14 in [28]), where however it was inferred that increasing bisection iterations would identify also corner points where $\psi(\vartheta)$ is not differentiable. This turns out to be not true, as Fig. 6 shows. The right panel depicts $\psi(\vartheta)$ obtained by postprocessing all grid points obtained by the proposed scheme (tested on the model described in Sec. VIII-A), showing the

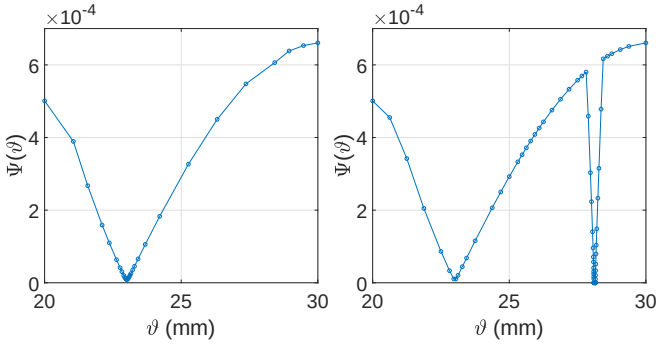

Fig. 6: Left: parameter sampling based on the bisection of $\psi(\vartheta)$ as in [28]. Right: $\psi(\vartheta)$ is computed for all parameter grid points resulting from proposed perturbation approach.

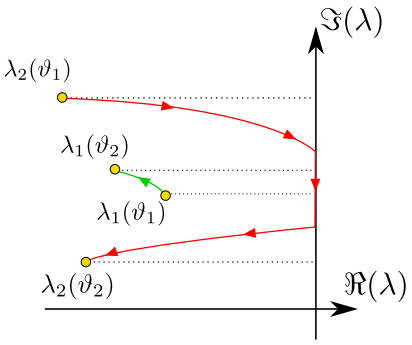

Fig. 7: SHH eigenvalue trajectories corresponding to the example of Fig. 6 (picture not to scale).

onset of a sharp passivity violation region (characterized by $\psi(\vartheta) = 0$) with a very small footprint in the parameter space. This violation is missed completely using the check proposed in [28], which relies on the smoothness of $\psi(\vartheta)$ (left panel). Figure 7 provides another illustration of this case by depicting the trajectories of the two SHH eigenvalues closest to the imaginary axis as ϑ sweeps in an interval $[\vartheta_1, \vartheta_2]$ which encapsulates the narrow violation region. The check in [28] detects only the slowly varying trajectory of λ_1, which remains far from the imaginary axis, and misses the trajectory of λ_2 which undergoes a fast transition from ϑ_1 to ϑ_2 hitting the imaginary axis. The proposed full-spectrum perturbation approach is able to detect the faster "speed" of λ_2, thus tracking its trajectory and spotting the small passivity violation.

VII. Passivity Enforcement

We now describe our proposed multivariate passivity enforcement scheme. We assume that $\mathbf{H}(s, \boldsymbol{\vartheta})$ is detected as non-passive in some regions $\Theta_\alpha \subset \Theta$ for $\alpha = 1, 2, \ldots$ (delimited by the red/green boundaries in Fig. 5). We seek for a perturbed model

$$\widehat{\mathbf{H}}(s, \boldsymbol{\vartheta}) = \mathbf{H}(s, \boldsymbol{\vartheta}) + \Delta\mathbf{H}(s, \boldsymbol{\vartheta}) \tag{22}$$

that is uniformly passive $\forall \boldsymbol{\vartheta} \in \Theta$. We define the model perturbation based on the parameterization scheme (2) as

$$\Delta\mathbf{H}(s; \boldsymbol{\vartheta}) = \Delta\mathbf{C}(\boldsymbol{\vartheta}) \left(s\mathbf{E} - \mathbf{A}(\boldsymbol{\vartheta})\right)^{-1} \mathbf{B} \tag{23}$$

with

$$\Delta\mathbf{C}(\boldsymbol{\vartheta}) = \sum_{\ell=1}^{\bar{\ell}} \Delta\mathbf{C}_\ell \, \xi_\ell(\boldsymbol{\vartheta}), \tag{24}$$

where the decision variables are the perturbations $\Delta\mathbf{C}_\ell$ in the coefficients of the parameter-dependent state-output map, which we collect in matrix $\mathbf{X} = (\Delta\mathbf{C}_1, \ldots, \Delta\mathbf{C}_{\bar{\ell}})$. This choice provides the natural generalization of widespread non-parametric passivity enforcement schemes [6], [41]. The system poles are preserved, since the dynamic matrix $\mathbf{A}(\boldsymbol{\vartheta})$ is left unchanged. This choice is appropriate since most common realization schemes collect the (parameter-dependent) residues of a pole-residue or barycentric form of $\mathbf{H}(s, \boldsymbol{\vartheta})$ in matrix $\mathbf{C}(\boldsymbol{\vartheta})$, see [19]. Matrix $\Delta\mathbf{H}(s, \boldsymbol{\vartheta})$ can be equivalently written as

$$\Delta\mathbf{H}(s, \boldsymbol{\vartheta}) = \mathbf{X} \cdot \mathbf{Z}(s, \boldsymbol{\vartheta}), \tag{25}$$

with

$$\mathbf{Z}(s, \boldsymbol{\vartheta}) = \left\{ [\xi_1(\boldsymbol{\vartheta}), \ldots, \xi_{\bar{\ell}}(\boldsymbol{\vartheta})]^\mathsf{T} \otimes \mathbf{I}_{\bar{\mathrm{N}}} \right\} [s\mathbf{E} - \mathbf{A}(\boldsymbol{\vartheta})]^{-1}\mathbf{B}$$

and where $\otimes$ denotes the matrix Kronecker product.

A. Preserving model accuracy

In order to keep the perturbed model responses as accurate as possible, we minimize the perturbation amount $\|\Delta\mathbf{H}(s_\kappa, \boldsymbol{\vartheta}_\kappa)\|$ at $\kappa = 1, \ldots, \bar{\kappa}$ prescribed points in the frequency-parameter space. These points may coincide with (or be a subset of) the original data points that were used to extract the initial model. Model accuracy is preserved by minimizing the following cost function

$$\mathbf{F}(\mathbf{x}) = \sum_{\kappa=1}^{\bar{\kappa}} \|\mathbf{X} \cdot \mathbf{Z}(s_\kappa, \boldsymbol{\vartheta}_\kappa)\|_F^2, \quad \mathbf{x} = \mathrm{vec}(\mathbf{X}) \tag{26}$$

which is based on the Frobenius $_F$ norm. Other norm choices including weighted norms are possible as in standard non-parameterized passivity enforcement methods [6], [41], [42].

B. Formulating local passivity constraints

While minimizing (26), the passivity conditions detailed in Sec. III must be enforced. This is possible by exploiting the worst-case passivity violation information $\mathcal{W}_\mu$, $\mu = 1 \ldots, \bar{\mu}$, available from the passivity check discussed in Sec. VI.

1) Immittance representations: Consider the worst-case passivity violation $\mathcal{W}_\mu = \{\bar{\omega}_\mu, \bar{\boldsymbol{\vartheta}}_\mu; \bar{\lambda}^\mu_{\min}\}$, where $\bar{\lambda}^\mu_{\min} < 0$. Applying a first-order eigenvalue perturbation to $\boldsymbol{\Psi}_I(\mathrm{j}\omega, \boldsymbol{\vartheta})$, centered at $(\bar{\omega}_\mu, \bar{\boldsymbol{\vartheta}}_\mu)$, to selectively modify the negative eigenvalue $\bar{\lambda}^\mu_{\min}$, we can write

$$\widehat{\lambda}^\mu_{\min} = \bar{\lambda}^\mu_{\min} + 2\ \Re\{\mathbf{v}_\mu^\mathsf{H} \Delta\mathbf{H}(\mathrm{j}\bar{\omega}_\mu, \bar{\boldsymbol{\vartheta}}_\mu)\mathbf{v}_\mu\}, \tag{27}$$

where $\mathbf{v}_\mu$ is the right eigenvector of $\mathbf{H}(\mathrm{j}\bar{\omega}_\mu, \bar{\boldsymbol{\vartheta}}_\mu)$ associated with $\bar{\lambda}^\mu_{\min}$. After few simple algebraic manipulations we can write

$$\widehat{\lambda}^\mu_{\min} = \bar{\lambda}^\mu_{\min} + \mathbf{y}_\mu^\mathsf{T} \cdot \mathbf{x} \tag{28}$$

with

$$\mathbf{y}_\mu^\mathsf{T} = 2\ \Re\{[\mathbf{Z}(\mathrm{j}\bar{\omega}_\mu, \bar{\boldsymbol{\vartheta}}_\mu)\, \mathbf{v}_\mu]^\mathsf{T} \otimes \mathbf{v}_\mu^\mathsf{H}\}. \tag{29}$$

Enforcing now $\widehat{\lambda}^\mu_{\min} \geq 0$ as required by (6) leads to the following linear inequality constraint

$$-\mathbf{y}_\mu^\mathsf{T} \cdot \mathbf{x} \leq \bar{\lambda}^\mu_{\min} \tag{30}$$

to be enforced for all μ local violations.

2) Scattering representations: For scattering representations we start with the worst-case passivity violations $\mathcal{W}_\mu = \{\bar{\omega}_\mu, \bar{\boldsymbol{\vartheta}}_\mu; \bar{\sigma}^\mu_{\max}\}$, where $\bar{\sigma}^\mu_{\max} > 1$. These singular values are perturbed to enforce condition (8). Applying again a first-order singular value perturbation centered at $(\bar{\omega}_\mu, \bar{\boldsymbol{\vartheta}}_\mu)$ to $\mathbf{H}(\mathrm{j}\omega, \boldsymbol{\vartheta})$ leads to

$$\widehat{\sigma}^\mu_{\max} = \bar{\sigma}^\mu_{\max} + \Re\{\mathbf{u}_\mu^\mathsf{H} \Delta\mathbf{H}(\mathrm{j}\bar{\omega}_\mu, \bar{\boldsymbol{\vartheta}}_\mu)\mathbf{v}_\mu\} \tag{31}$$

where $\mathbf{u}_\mu$, $\mathbf{v}_\mu$ are the left and right singular vectors of $\mathbf{H}(\mathrm{j}\bar{\omega}_\mu, \bar{\boldsymbol{\vartheta}}_\mu)$ associated with $\bar{\sigma}^\mu_{\max}$. Expressing (31) in terms of our decision variables as

$$\widehat{\sigma}^\mu_{\max} = \bar{\sigma}^\mu_{\max} + \mathbf{z}_\mu^\mathsf{T} \cdot \mathbf{x} \tag{32}$$

with

$$\mathbf{z}_\mu^\mathsf{T} = \Re\{[\mathbf{Z}(\mathrm{j}\bar{\omega}_\mu, \bar{\boldsymbol{\vartheta}}_\mu)\, \mathbf{v}_\mu]^\mathsf{T} \otimes \mathbf{u}_\mu^\mathsf{H}\} \tag{33}$$

leads to the linear inequality constraint

$$\mathbf{z}_\mu^\mathsf{T} \cdot \mathbf{x} \leq 1 - \bar{\sigma}^\mu_{\max} \tag{34}$$

that must be enforced for all μ.

C. Collecting and enforcing local passivity constraints

Defining now

$$\mathbf{g}_\mu = -\mathbf{y}_\mu, \qquad h_\mu = \bar{\lambda}^\mu_{\min} \qquad \text{immittance,} \tag{35}$$

$$\mathbf{g}_\mu = \mathbf{z}_\mu, \qquad h_\mu = 1 - \bar{\sigma}^\mu_{\max} \qquad \text{scattering,} \tag{36}$$

we can formulate our multivariate passivity enforcement problem as

$$\min_{\mathbf{x}} \mathbf{F}(\mathbf{x}), \quad \text{s.t. } \mathbf{g}_\mu^\mathsf{T} \cdot \mathbf{x} - h_\mu \leq 0, \quad \mu = 1, \ldots, \bar{\mu} \tag{37}$$

Due to the linearity of (26), implying that $\mathbf{F}(\mathbf{x})$ is quadratic in the decision variables, the above problem is convex and is readily solved with standard methods [43].

As in non-parameterized passivity enforcement schemes, the passivity constraints are only finite and are not exact, since based on a first-order approximation. Therefore, the optimization problem (37) is formulated by repeating the passivity characterization and solved iteratively until a uniformly passive model is obtained, i.e., the set $\mathcal{W}$ is empty. We denote these as "outer" iterations.

A high-level description of the proposed passivity enforcement scheme is reported in Algorithm (1), where the distinction between outer iterations (for passivity enforcement) and inner iterations (for passivity characterization at each outer iteration) can be appreciated.

Algorithm 1 Multi-variate passivity enforcement

Require: Initial parameterized model in form (1)
repeat (outer passivity enforcement iterations)
  Evaluate SHH eigenvalues at initial grid points
  Initialize local passivity violations $\mathcal{W}$
  for $J = 1, \ldots, J_{\max}$ (inner refinement iterations) **do**
    Determine which cells must be refined
    if some cells must be refined **then**
      Refine cells
      Compute SHH eigs at new points
      Update $\mathcal{W}$
    else
      break
    end if
  end for
  if $\mathcal{W} \neq \emptyset$ (model is not passive) **then**
    Assemble local passivity constraints and solve (37)
    Update model coefficients
  end if
until $\mathcal{W} = \emptyset$ (model is passive)
return Passive model $\widehat{\mathbf{H}}(s, \boldsymbol{\vartheta})$

D. Some remarks about convergence

The proposed approach extends to the multi-parameter case one of the well-established passivity enforcement schemes available for non-parameterized models [6], [27]. Although this scheme is widely used since implemented in several commercial CAD tools, no proof of convergence exists even in the non-parameterized case. Therefore, we are not able to provide a proof of convergence of the proposed extended parameterized scheme. In this Section, we provide a theoretical justification of the main heuristics on which we base our numerical implementation, whose convergence was always observed in all test cases that we analyzed so far. This is of course not a proof, whose completion is still an open problem.

Consider a state-space model with constant $\mathbf{A}, \mathbf{C}$ obtained from (1) by removing parameter dependence. Assuming the model is not passive, we perturb it as in (23), where now $\Delta\mathbf{C}$ is a constant perturbation applied to $\mathbf{C}$. The cost function to be minimized in order to guarantee optimal accuracy is still (26), where $\mathbf{Z}$ is only evaluated at s_κ. We denote as $\mathbf{H}(s;\mathbf{x})$ the dependence of the model on the decision variables $\mathbf{x}$ (elements of $\Delta\mathbf{C}$). This dependence, coherently with (23), is affine.

Assuming a scattering representation (the same can be extended to the immittance case), a known convex formulation [44] of the passivity enforcement problem is

$$\min_{\mathbf{x}} \mathbf{F}(\mathbf{x}), \quad \text{s.t. } \|\mathbf{H}(s;\mathbf{x})\|_{\mathcal{H}_\infty} \leq 1 \tag{38}$$

where

$$\|\mathbf{H}(s;\mathbf{x})\|_{\mathcal{H}_\infty} = \sup_{\omega\in\mathbb{R}} \sigma_{\max}(\mathbf{H}(\mathrm{j}\omega;\mathbf{x})) \tag{39}$$

Since convex, the optimal solution (the most accurate passive model) is attained through any convex optimization solver. However, as discussed in [44], the constraint (38) in terms of the $\mathcal{H}_\infty$ norm defines a feasible set with non-smooth boundaries, thus requiring subgradient formulations that, although with provable convergence, require an impractical number of iterations (in the order of hundreds or thousands, even for very simple low-order cases).

The lack of smoothness is due to the "sup" operator in (39). However, each individual singular value trajectory $\sigma_i(\mathrm{j}\omega;\mathbf{x})$ is smooth due to the assumed asymptotic stability. Therefore, an equivalent (smooth) formulation of (38) is obtained as

$$\min_{\mathbf{x}} \mathbf{F}(\mathbf{x}), \quad \text{s.t. } \sigma_i(\mathbf{H}(\mathrm{j}\omega;\mathbf{x})) \leq 1, \forall i\ \forall\omega \in \mathbb{R}. \tag{40}$$

Since equivalent to (38), also (40) is convex and its optimal solution can in principle be computed with a proper convex solver. However, the passivity constraint is ∞-dimensional since formulated on the entire real line. Since all singular values are smooth hence continuous, a further equivalent formulation can be derived as

$$\min_{\mathbf{x}} \mathbf{F}(\mathbf{x}), \quad \text{s.t. } \bar{\sigma}_i(\mathbf{H}(\mathrm{j}\bar{\omega}_{i,k};\mathbf{x})) \leq 1, \forall i,k \tag{41}$$

where $\bar{\omega}_{i,k}$ denotes the frequency where the k-th local maximum of the i-th singular value occurs, and (i,k) span all such local maxima (including possibly $\omega = \infty$). So, if *all* local maxima are identified, the formulation (41) is equivalent to (38) and thus convex. Theorems 1 and 2 in Sec. V guarantee that (in the non-parameterized case) all local maxima are identified and computed algebraically.

At this stage we introduce some approximations, loosing the possibility (to the best of Authors' knowledge) to prove formal convergence.

- First, we linearize all the constraints (41) through a first-order singular value perturbation a analysis, as in (31). Enforcing a single such linear constraint instead of (41) is roughly equivalent to performing a single Newton iteration, where the descent direction on $\mathbf{x}$ is such that the corresponding singular value (which is larger than one) is decreased.
- Instead of running a Newton iteration with a single descent direction, we impose *all* constraints (41) at the same time, leaving to the convex solver the role of computing the descent direction that *at the same time* decreases the value of all singular value maxima. The concurrent constraints used in our approach thus include at least all vertices whose convex hull defines the subdifferential of the $\mathcal{H}_\infty$ norm, whereas the provably converging schemes of [44] adopt a descent direction by picking any subgradient, i.e., any single vector in the above subdifferential. These more aggressive concurrent constraints enable (non-provable) convergence in usually less than ten iterations, compared to the several hundreds/thousands of [44].
- Clearly, there is no guarantee that decreasing locally all the maxima will not generate new maxima at the next iteration, located at different frequencies. For this reason, our scheme embeds the so-called "robust iterations" (see [45], [46]), which instead of solving (41) iteratively, performs a number r of iterations (typically $r = 1$ or 2), evaluates the location of new local maxima if any, and repeats the same iteration by adding local constraints also at the corresponding new frequencies. This scheme, detailed

in [6, Sec. 10.10.5], proves very effective in avoiding the emergence of new passivity violations as the iterations progress.
- In any case, due to the linearization (31), the problem that is solved at each iteration is not fully equivalent to (41), and therefore outer iterations are required.

On top of the above considerations, the proposed parameterized passivity enforcement scheme needs a further adaptive sampling in the parameter space. Although particular care has been taken in its formulation based on the SHH eigenspectrum sensitivities, the number of points that can be sampled remains only finite, and the prediction/interpolation criteria to infer that there are no undetected violations are only based on first-order approximations. This is why we are not able to prove global convergence.

VIII. Examples

In this Section we will provide some numerical results of the proposed passivity verification and enforcement methods, applied to various test cases. All results were obtained using a standard laptop (Intel Core-i7 2.3 GHz CPU with 16 GB of RAM), using a prototypal MATLAB implementation.

A. Partially coupled multi-conductor line

We start with a single-parameter ($\rho = 1$) electrical interconnect structure made of 3 adjacent differential pairs, each composed of two parallel circular wires (length 10 cm, center-to-center distance 1.61 mm) forming a 6-wire multi-conductor transmission line. The differential pairs are considered to be electromagnetically coupled only over a length $\vartheta = L_c$, which is our free parameter $\vartheta \in \Theta = [20,\ 40]$ mm. More details on this structure are available in [28].

An initial parameterized model ($\bar{n} = 30$, $\bar{\ell} = 5$) was computed using the PSK iteration [29], [31] applied to a set of 11 frequency responses (linearly spaced in Θ), each including $\bar{k} = 500$ samples in the range [1 Hz, 5 GHz]. Since this initial model is not passive, we applied our proposed algorithm, which produced a passive model in 12 iterations. As Fig. 8 shows for one representative response, the passive model closely matches the initial data from which the model was derived (worst-case relative RMS error $13 \cdot 10^{-3}$).

The right panel of Fig. 6 depicts the results of proposed adaptive sampling (using $J_{\max} = 10$) applied to the model resulting from the passivity enforcement method as implemented in [28]. This model is still not passive, due to the presence of a small localized violation identified by a vanishing distance of the SHH eigenspectrum from the imaginary axis. Compared to the left panel of Fig. 6, based on [28] which is seen to miss a localized passivity violation area, our new approach proves much more reliable.

B. A parameterized multi-board interconnect

We now turn to a 2D example ($\rho = 2$), consisting of a high-speed multi-board link that connects two multilayer PCBs [47] through a connector, including vertical vias for routing through the inner PCB layers. The parameters of interest are the via pad (ϑ^1) and anti-pad (ϑ^2) radii varying, respectively, in the ranges $[100,\ 300]$ and $[400,\ 600]$ μm. An initial model ($\bar{n} = 24$, $\bar{\ell}_1 = \bar{\ell}_2 = 3$) was computed via the PSK iteration starting from discrete scattering frequency samples (courtesy of Prof. C. Schuster and Dr. J. Preibisch, Technische Universität Hamburg-Harburg, Hamburg, Germany) spanning the band $[0, 5]$ GHz. The worst-case relative RMS error of this model among all the port responses is $14 \cdot 10^{-3}$.

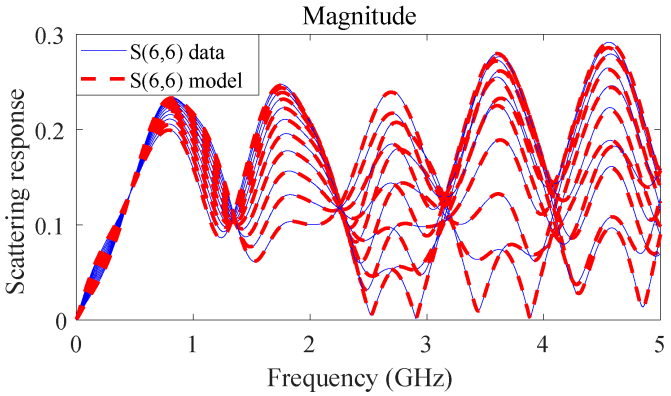

Fig. 8: Comparison between passive model and raw data for one representative response $S_{6,6}(\mathrm{j}\omega;\vartheta)$ of the partially coupled interconnect of Sec. VIII-A. The various response pairs correspond to a linear sweep on ϑ in its range.

The initial model is not passive, as the top-left panel of Fig. 9 confirms by highlighting with red dots the points in the 2D parameter space that are adaptively processed by our proposed algorithm ($J_{\max} = 8$), and for which at least one imaginary SHH eigenvalue is detected. The other panels in Fig. 9 depict the evolution of the passivity violation areas (red) through iterations of our proposed enforcement algorithm. After 5 iterations (requiring 12 minutes) the model becomes passive, with a worst-case relative RMS error $14 \cdot 10^{-3}$, which is essentially preserved through the iterations. The two panels in Fig. 10 compare the responses of the passive model to the initial data by sweeping one parameter at the time while keeping the other fixed. Almost no difference is visible in these plots between model and data, confirming the effectiveness of the adopted cost function (26) for accuracy preservation.

C. A transmission-line network

The last example is a transmission-line network made of four cascaded lossy line segments with three internal loaded stubs. We consider two different parameterizations (respectively, 2D and 3D) for this structure. Initially we parameterize just the central stub and its adjacent line lengths, that vary, respectively, in $\vartheta^1 \in [5,\ 7]$ mm and $\vartheta^2 \in [9,\ 10]$ mm. A three-dimensional case is obtained by parameterizing also the central stub load by means of its reflection coefficient $\vartheta^3 \in [0.1,\ 0.5]$, and restricting the range of ϑ^1 to $[6,\ 7]$ mm (the original range led to a first-pass passive model, for which no relevant results could be shown). All other line and stub lengths are fixed to their nominal values (7 mm for the direct lines and 1 mm for the stubs). The non-parameterized loads reflection coefficients are fixed to 0.5.

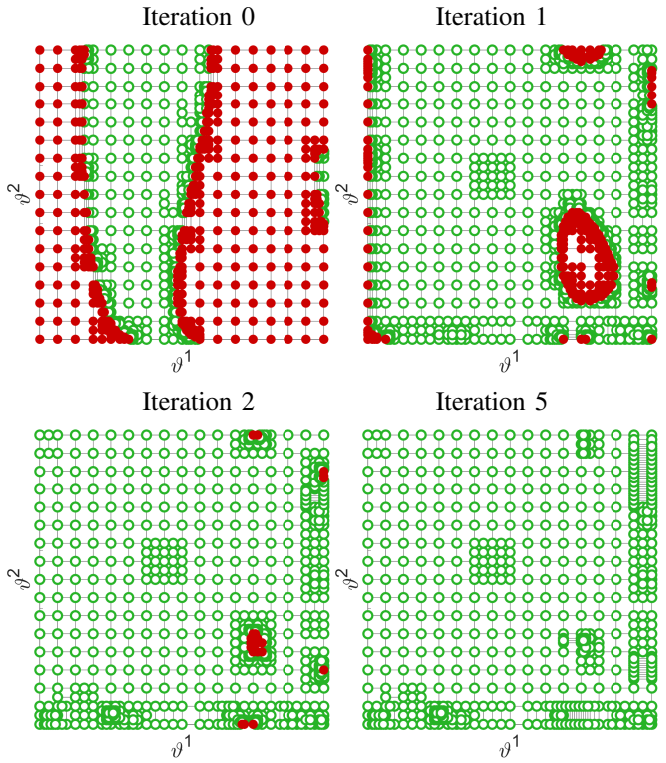

Fig. 9: Passivity characterization of the multiboard interconnect model illustrated after successive passivity enforcement (outer) iterations. Empty green (filled red) dots highlight passive (non-passive) parameter values for which no (some) SHH eigenvalues are detected by the proposed adaptive sampling algorithm.

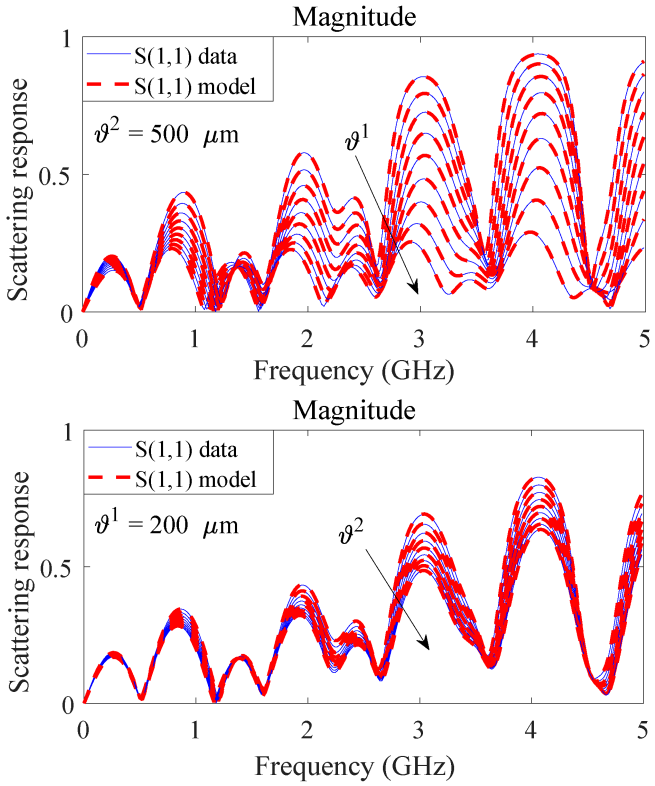

Fig. 10: Model responses compared to raw data for the multiboard interconnect parameterized by via pad (ϑ^1) and antipad (ϑ^2) radii.

We extracted two initial models ($\bar{n} = 20$, $\bar{\ell}_1 = \bar{\ell}_2 = 3$ and $\bar{n} = 20$, $\bar{\ell}_1 = \bar{\ell}_2 = 3$, $\bar{\ell}_3 = 2$, respectively) from scattering responses, sampled both in the parameter space and along frequency over a band [1 Hz, 10 GHz], obtained with a frequency-domain 2D integral field solver combined with a transmission-line solver. The worst-case RMS relative error of this initial model with respect to available validation data is $46.2 \cdot 10^{-3}$ and $22.6 \cdot 10^{-3}$ for bi- and tri-variate models, respectively.

Both initial models are not passive (see Fig. 11). We thus enforce their passivity with the proposed method ($J_{\max} = 8$ and $J_{\max} = 6$ for bi- and tri-variate models, respectively). The bi-variate passive model is obtained in 9 iterations (22 minutes), while just 1 iteration (20 minutes) is required to compensate the small violation occurring in the tri-variate case (see Fig. 11). Figures 12a-b compare the responses of the final passive bi-variate model to the original data used for model extraction for fixed $\vartheta^1 = 6.1$ mm and $\vartheta^2 = 9.5$ mm while sweeping ϑ^2 and ϑ^1, respectively. The same comparison is done for the tri-variate model, as shown in Fig. 12c-d, for fixed $\vartheta^1 = 6.4$ mm, $\vartheta^3 = 0.26$ and $\vartheta^1 = 6.4$ mm, $\vartheta^2 = 9.4$ mm, while sweeping ϑ^2 and ϑ^3, respectively. Also in this case the models accuracy is preserved, with a final RMS error $46.2 \cdot 10^{-3}$ and $22.7 \cdot 10^{-3}$ for the bi- and tri-variate models, respectively.

D. Computational Times

We finally compare the performance of proposed algorithm to the method in [28], for those cases for which this comparison can be performed (i.e., single-parameter models with $\rho = 1$). Figure 13 compares the runtime required by the two approaches for passivity enforcement applied to 8 different test cases. We see that the CPU times of the proposed approach (orange bars) are comparable to (and in few cases lower than) those of [28] (empty bars). Hence, the mentioned reliability improvement of this new Hamiltonian-based adaptive sampling scheme does not come with extra costs in terms of efficiency.

In some limited cases, the proposed algorithm may lead to a slightly larger runtime than [28]. This occurs for nearly lossless passive systems, which are characterized by SHH eigenvalues that occur in clusters very close to the imaginary axis. These cases do require a more aggressive sampling, and the extra cost is tolerable in order to avoid missing important passivity violations, as in Fig. 6.

IX. Conclusions

In this paper, we presented a novel multi-variate passivity verification and enforcement approach. The proposed adaptive sampling scheme is based on first-order SHH eigenvalue perturbations that, combined with an ad-hoc tessellation of the parameter space, enable to efficiently verify and enforce

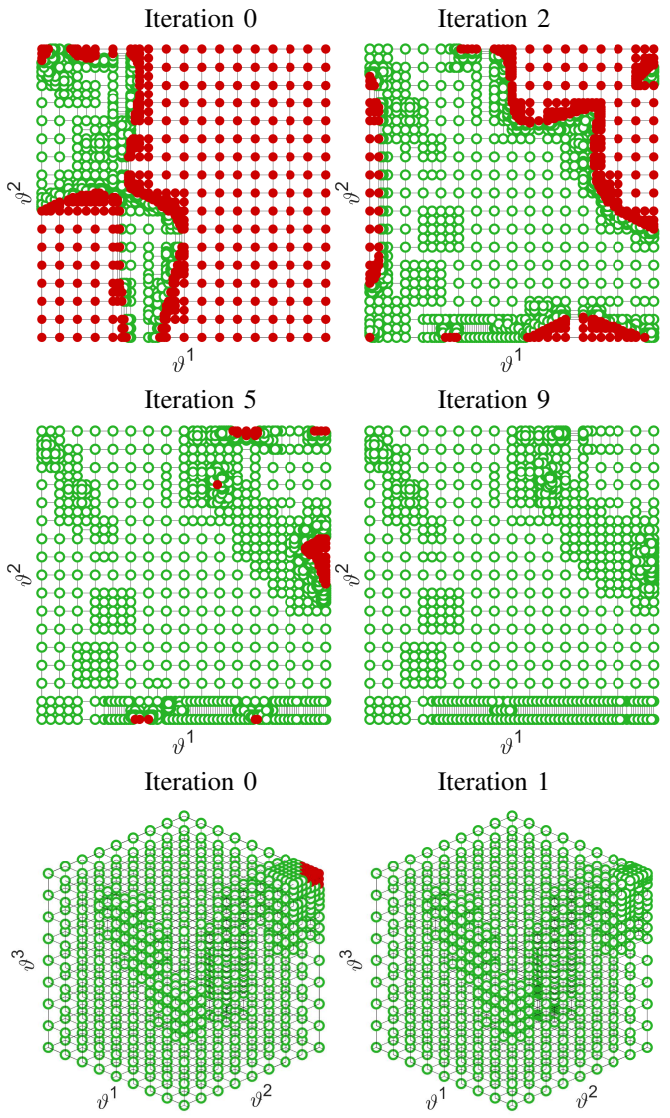

Fig. 11: As in Fig. 9, but for the transmission line network models. Panels (a)–(d) refers to the bi-variate model, while (e)–(f) show the parameter space for the tri-variate case.

passivity for multi-variate macromodels. The "predictive" aspect of this approach enables a considerable reliability improvement with respect to other existing schemes, with a comparable computational cost. The uniformly passive models obtained from our algorithm can be reliably used as blocks in system-level (transient) simulations in what-if, optimization and design centering flows, without the risk of incurring into numerical instabilities.

The proposed algorithm is not expected to be the ultimate solution to the multivariate passivity verification and enforcement problem. Due to the structure of the parameter space, a major drawback of proposed strategy is still related to its complexity, that grows exponentially with the number of parameters despite the aggressive adaptive sampling scheme that is adopted. Although the formulation is general, practical applicability of this method is granted only up to 2-3 independent parameters. Embedding higher-dimensional

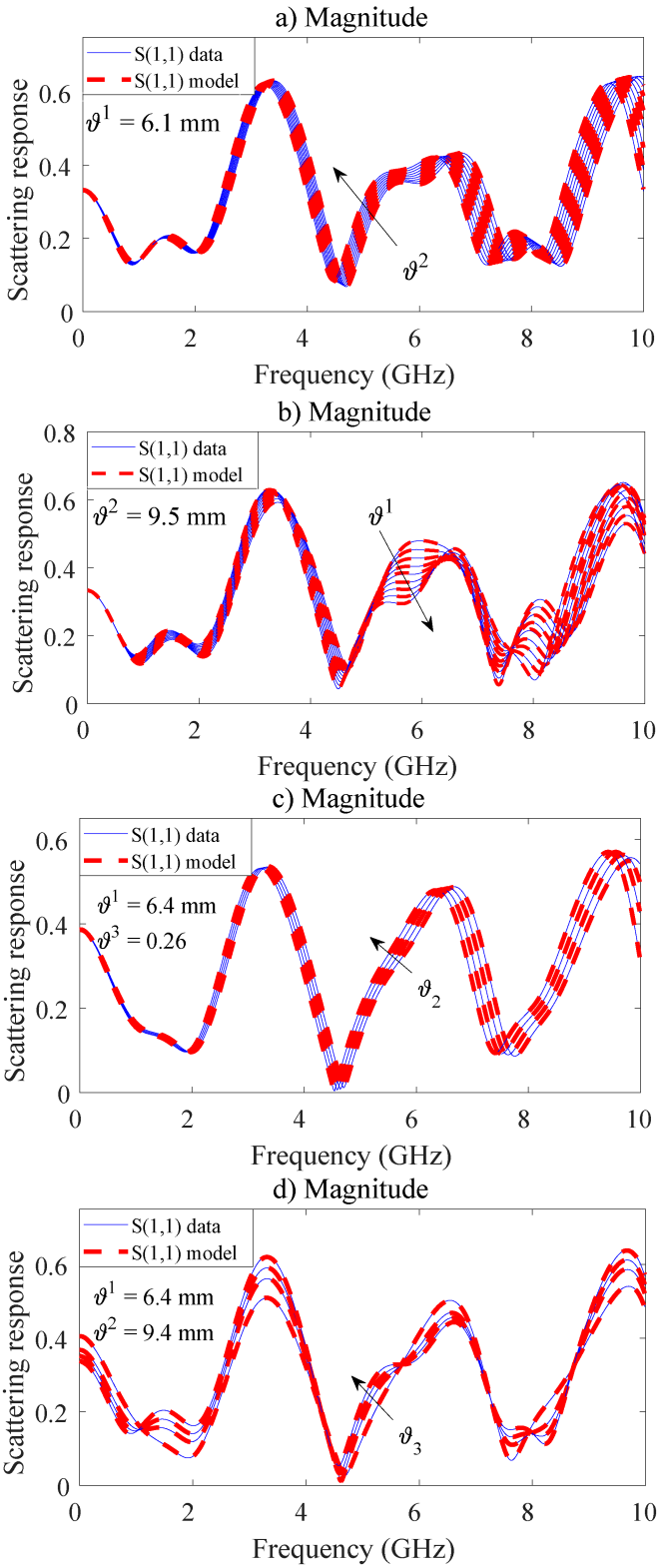

Fig. 12: a) and b): comparison between original data and passive model responses for the bi-variate transmission line model, parameterized by stub and line lengths, ϑ^1 and ϑ^2 respectively; c) and d) same for the tri-variate transmission line model, parameterized by stub and line lengths (ϑ^1, ϑ^2 respectively) and load reflection coefficient ϑ^3

.

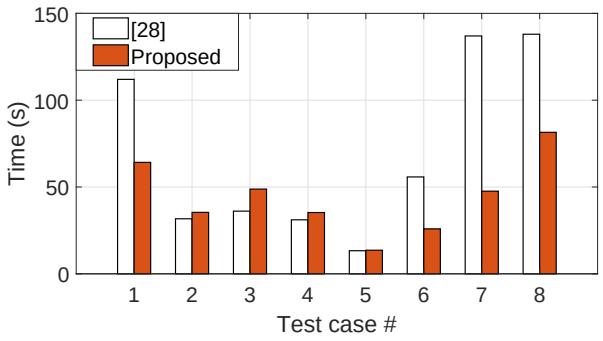

Fig. 13: Runtime of proposed passivity enforcement scheme (orange bars) compared to [28] (empty bars).

parameterizations in a closed form into a black-box reduced-order model in a data-driven setting will require different approaches. Our future work will thus be focused on reducing this complexity by possibly exploiting structure and/or smoothness properties in the parameter space, aiming at model generation and passivity verification/enforcement at least with polynomial complexity. The goal of this research line remains the fully automated generation of robust, passive and accurate behavioral models in a high-dimensional multivariate setting.

REFERENCES

[1] M. Swaminathan, D. Chung, S. Grivet-Talocia, K. Bharath, V. Laddha, and J. Xie, "Designing and modeling for power integrity," *IEEE Transactions on Electromagnetic Compatibility*, vol. 52, no. 2, pp. 288–310, May 2010.

[2] R. Achar and M. S. Nakhla, "Simulation of high-speed interconnects," *Proceedings of the IEEE*, vol. 89, no. 5, pp. 693–728, May 2001.

[3] P. Benner, M. Hinze, and E. J. W. ter Maten, *Model reduction for circuit simulation*. Springer, 2010, vol. 74.

[4] B. Gustavsen and A. Semlyen, "Application of vector fitting to state equation representation of transformers for simulation of electromagnetic transients," *Power Delivery, IEEE Transactions on*, vol. 13, no. 3, pp. 834–842, jul 1998.

[5] B. Gustavsen, "Wide band modeling of power transformers," *Power Delivery, IEEE Transactions on*, vol. 19, no. 1, pp. 414–422, jan. 2004.

[6] S. Grivet-Talocia and B. Gustavsen, *Passive macromodeling: Theory and applications*. John Wiley & Sons, 2015, vol. 239.

[7] W. H. A. Schilders, H. A. Van Der Vorst, and J. Rommes, *Model order reduction: theory, research aspects and applications*. Springer Verlag, 2008.

[8] A. C. Antoulas, *Approximation of large-scale dynamical systems*. Society for Industrial and Applied Mathematics, 2005.

[9] S. X. D. Tan and L. He, *Advanced Model Order Reduction Techniques in VLSI Design*. Cambridge University Press, New York, 2007.

[10] A. Odabasioglu, M. Celik, and L. T. Pileggi, "PRIMA: Passive reduced-order interconnect macromodeling algorithm," *IEEE transactions on computer-aided design of integrated circuits and systems*, vol. 17, no. 8, pp. 645–654, 1998.

[11] E. J. Grimme, "Krylov projection methods for model reduction," Ph.D. thesis, Univ. Illinois Urbana Champaign, Tech. Rep., 1997.

[12] B. Moore, "Principal component analysis in linear systems: Controllability, observability, and model reduction," *Automatic Control, IEEE Transactions on*, vol. 26, no. 1, pp. 17–32, feb 1981.

[13] K. Glover, "All optimal Hankel-norm approximations of linear multivariable systems and their L_∞ error bounds," *International Journal of Control*, vol. 39, no. 6, pp. 1115–1193, 1984.

[14] J. R. Phillips and L. M. Silveira, "Poor man's TBR: a simple model reduction scheme," *Computer-Aided Design of Integrated Circuits and Systems, IEEE Transactions on*, vol. 24, no. 1, pp. 43–55, 2005.

[15] B. Gustavsen and A. Semlyen, "Rational approximation of frequency domain responses by vector fitting," *Power Delivery, IEEE Transactions on*, vol. 14, no. 3, pp. 1052–1061, jul 1999.

[16] A. J. Mayo and A. C. Antoulas, "A framework for the solution of the generalized realization problem," *Linear algebra and its applications*, vol. 425, no. 2-3, pp. 634–662, 2007.

[17] S. Lefteriu and A. C. Antoulas, "A new approach to modeling multiport systems from frequency-domain data," *Computer-Aided Design of Integrated Circuits and Systems, IEEE Transactions on*, vol. 29, no. 1, pp. 14–27, jan. 2010.

[18] M. Kabir and R. Khazaka, "Macromodeling of distributed networks from frequency-domain data using the loewner matrix approach," *IEEE Transactions on Microwave Theory and Techniques*, vol. 60, no. 12, pp. 3927–3938, 2012.

[19] P. Triverio, S. Grivet-Talocia, and M. S. Nakhla, "A parameterized macromodeling strategy with uniform stability test," *IEEE Trans. Advanced Packaging*, vol. 32, no. 1, pp. 205–215, Feb 2009.

[20] S. Grivet-Talocia and E. Fevola, "Compact parameterized black-box modeling via fourier-rational approximations," *IEEE Transactions on Electromagnetic Compatibility*, vol. 59, no. 4, pp. 1133–1142, 2017.

[21] A. Ionita and A. Antoulas, "Data-driven parametrized model reduction in the loewner framework," *SIAM Journal on Scientific Computing*, vol. 36, no. 3, pp. A984–A1007, 2014.

[22] F. Ferranti, L. Knockaert, and T. Dhaene, "Parameterized s-parameter based macromodeling with guaranteed passivity," *IEEE Microwave and Wireless Components Letters*, vol. 19, no. 10, pp. 608–610, 2009.

[23] F. Ferranti, L. Knockaert, T. Dhaene, and G. Antonini, "Passivity-preserving parametric macromodeling for highly dynamic tabulated data based on lur'e equations," *IEEE Transactions on Microwave Theory and Techniques*, vol. 58, no. 12, pp. 3688–3696, 2010.

[24] F. Ferranti, L. Knockaert, and T. Dhaene, "Passivity-preserving parametric macromodeling by means of scaled and shifted state-space systems," *IEEE Transactions on Microwave Theory and Techniques*, vol. 59, no. 10, pp. 2394–2403, 2011.

[25] F. Ferranti, T. Dhaene, and L. Knockaert, "Compact and passive parametric macromodeling using reference macromodels and positive interpolation operators," *Components, Packaging and Manufacturing Technology, IEEE Transactions on*, vol. 2, no. 12, pp. 2080–2088, Dec 2012.

[26] E. R. Samuel, L. Knockaert, F. Ferranti, and T. Dhaene, "Guaranteed passive parameterized macromodeling by using sylvester state-space realizations," *IEEE Transactions on Microwave Theory and Techniques*, vol. 61, no. 4, pp. 1444–1454, 2013.

[27] S. Grivet-Talocia and A. Ubolli, "A comparative study of passivity enforcement schemes for linear lumped macromodels," *IEEE Trans. Advanced Packaging*, vol. 31, no. 4, pp. 673–683, Nov 2008.

[28] Grivet-Talocia, Stefano, "A perturbation scheme for passivity verification and enforcement of parameterized macromodels," *IEEE Transactions on Components, Packaging and Manufacturing Technology*, vol. 7, no. 11, pp. 1869–1881, 2017.

[29] S. Grivet-Talocia and R. Trinchero, "Behavioral, parameterized, and broadband modeling of wired interconnects with internal discontinuities," *IEEE Transactions on Electromagnetic Compatibility*, vol. 60, no. 1, pp. 77–85, 2018.

[30] A. Zanco, S. Grivet-Talocia, T. Bradde, and M. D. Stefano, "Multivariate macromodeling with stability and passivity constraints," in *2018 IEEE 22nd Workshop on Signal and Power Integrity (SPI)*, May 2018, pp. 1–4.

[31] C. Sanathanan and J. Koerner, "Transfer function synthesis as a ratio of two complex polynomials," *Automatic Control, IEEE Transactions on*, vol. 8, no. 1, pp. 56–58, jan 1963.

[32] M. R. Wohlers, *Lumped and Distributed Passive Networks*. Academic press, 1969.

[33] B. D. O. Anderson and S. Vongpanitlerd, *Network analysis and synthesis*. Prentice-Hall, 1973.

[34] Z. Zhang and N. Wong, "Passivity check of S-parameter descriptor systems via S-parameter generalized Hamiltonian methods," *Advanced Packaging, IEEE Transactions on*, vol. 33, no. 4, pp. 1034–1042, Nov 2010.

[35] ——, "An efficient projector-based passivity test for descriptor systems," *Computer-Aided Design of Integrated Circuits and Systems, IEEE Transactions on*, vol. 29, no. 8, pp. 1203–1214, Aug 2010.

[36] ——, "Passivity test of immittance descriptor systems based on generalized Hamiltonian methods," *Circuits and Systems II: Express Briefs, IEEE Transactions on*, vol. 57, no. 1, pp. 61–65, Jan 2010.

[37] S. Boyd, V. Balakrishnan, and P. Kabamba, "A bisection method for computing the H_∞ norm of a transfer matrix and related problems," *Mathematics of Control, Signals and Systems*, vol. 2, no. 3, pp. 207–219, 1989.

[38] J. H. Wilkinson, *The algebraic eigenvalue problem*. Clarendon Press, 1965.
[39] T. G. Kolda and B. W. Bader, "Tensor decompositions and applications," *SIAM review*, vol. 51, no. 3, pp. 455–500, 2009.
[40] Y. Wang, Z. Zhang, C.-K. Koh, G. Shi, G. K.-H. Pang, and N. Wong, "Passivity enforcement for descriptor systems via matrix pencil perturbation," *Computer-Aided Design of Integrated Circuits and Systems, IEEE Transactions on*, vol. 31, no. 4, pp. 532–545, April 2012.
[41] S. Grivet-Talocia, "Passivity enforcement via perturbation of hamiltonian matrices," *IEEE Transactions on Circuits and Systems I: Regular Papers*, vol. 51, no. 9, pp. 1755–1769, 2004.
[42] S. Grivet-Talocia and A. Ubolli, "Passivity enforcement with relative error control," *IEEE Trans. Microwave Theory and Techniques*, vol. 55, no. 11, pp. 2374–2383, November 2007.
[43] S. P. Boyd and L. Vandenberghe, *Convex optimization*. Cambridge University Press, 2004.
[44] G. Calafiore, A. Chinea, and S. Grivet-Talocia, "Subgradient techniques for passivity enforcement of linear device and interconnect macromodels," *IEEE Transactions on Microwave Theory and Techniques*, vol. 60, no. 10, pp. 2990–3003, October 2012.
[45] B. Gustavsen, "Computer code for rational approximation of frequency dependent admittance matrices," *Power Delivery, IEEE Transactions on*, vol. 17, no. 4, pp. 1093–1098, oct 2002.
[46] ——, "Fast passivity enforcement for pole-residue models by perturbation of residue matrix eigenvalues," *Power Delivery, IEEE Transactions on*, vol. 23, no. 4, pp. 2278–2285, Oct 2008.
[47] J. Preibisch, T. Reuschel, K. Scharff, J. Balachandran, B. Sen, and C. Schuster, "Exploring efficient variability-aware analysis method for high-speed digital link design using pce," *DesignCon, Jan*, 2017.

Alessandro Zanco received the Bachelor Degree in Electrical Engineering in 2015 and the Master degree in Mechathronic Engineering in 2018 from Politecnico di Torino, Torino, Italy. He is currently pursuing his Ph.D in Electrical, Electronics and Communication Engineering, at Politecnico di Torino. His research interests include black-box modeling for EMC, with special emphasis on parametric passivity verification and enforcement techniques.

He is co-recipient of the 2018 Best Paper Award of the IEEE INTERATIONAL SYMPOSIUM ON ELECTROMAGNETIC COMPATIBILITY.

Stefano Grivet-Talocia (M'98–SM'07–F'18) received the Laurea and Ph.D. degrees in electronic engineering from the Politecnico di Torino, Turin, Italy.

From 1994 to 1996, he was with the NASA/Goddard Space Flight Center, Greenbelt, MD, USA. He is currently a Full Professor of electrical engineering with the Politecnico di Torino. He co-founded the academic spinoff company IdemWorks in 2007, serving as the President until its acquisition by CST in 2016. He has authored over 150 journal and conference papers. His current research interests include passive macromodeling of lumped and distributed interconnect structures, model-order reduction, modeling and simulation of fields, circuits, and their interaction, wavelets, time-frequency transforms, and their applications.

Dr. Grivet-Talocia was a co-recipient of the 2007 Best Paper Award of the IEEE TRANSACTIONS ON ADVANCED PACKAGING. He received the IBM Shared University Research Award in 2007, 2008, and 2009. He was an Associate Editor of the IEEE TRANSACTIONS ON ELECTROMAGNETIC COMPATIBILITY from 1999 to 2001 and He is currently serving as Associate Editor for the IEEE TRANSACTIONS ON COMPONENTS, PACKAGING AND MANUFACTURING TECHNOLOGY. He was the General Chair of the 20th and 21st IEEE Workshops on Signal and Power Integrity (SPI2016 and SPI2017).

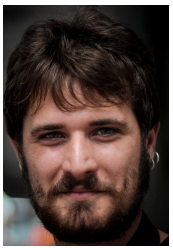

Tommaso Bradde received the Bachelor degree in Electronic Engineering from the Università degli studi Roma Tre, Rome ,Italy, in 2015 and the master degree in Mechatronic Engineering at Politecnico di Torino, Turin, Italy, in 2018. He is currently a Ph.D. student in Electrical, Electronics and Communication Engineering within the Politecnico di Torino. His current research is focused on data-driven parameterized macromodeling.

He is co-recipient of the 2018 Best Paper Award of the IEEE INTERATIONAL SYMPOSIUM ON ELECTROMAGNETIC COMPATIBILITY.

Marco De Stefano received the M.Sc. degree in mechatronic engineering from Politecnico di Torino, Torino, Italy, in 2018. He is currently pursuing his Ph.D. in Electrical, Electronics and Communication Engineering at the Politecnico di Torino. His research interests include model-order reduction, with emphasis on parameterized macromodeling, and fast simulation methods for signal and power integrity.

He is co-recipient of the 2018 Best Paper Award of the IEEE INTERATIONAL SYMPOSIUM ON ELECTROMAGNETIC COMPATIBILITY.